

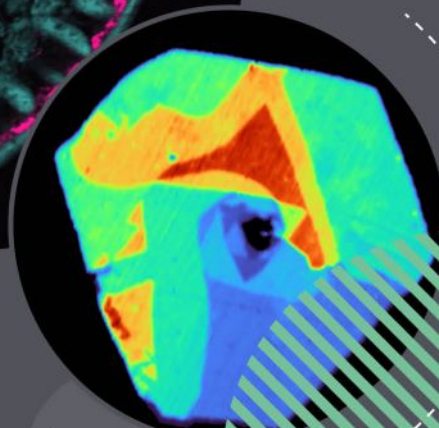


EDINBURGH
INSTRUMENTS

New eBook Out Now!



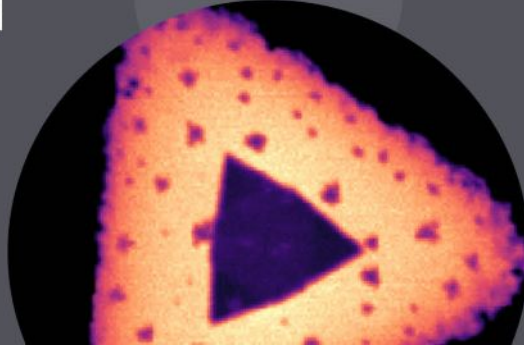
Scan to download
the new eBook...



Discover the ways we can enhance your research
with multiple techniques in one instrument

Multimodal Imaging Raman and Beyond

edinst.com



In situ high temperature Raman and DFT analysis of cerium fluoride and oxyfluoride structures in molten FLiNaK

Rongrong Cui  | Chenyang Wang 

Department of Radiochemistry, Shanghai Institute of Applied Physics, Chinese Academy of Sciences, Shanghai, China

Correspondence

Chenyang Wang, Department of Radiochemistry, Shanghai Institute of Applied Physics, Chinese Academy of Sciences, Shanghai 201800, China.
 Email: wangchenyang@sinap.ac.cn

Funding information

Strategic Priority Research Program of the Chinese Academy of Sciences, Grant/Award Number: XDA02030000; Frontier Science Key Program of the Chinese Academy of Sciences, Grant/Award Number: QYZDY-SSW-JSC016

Abstract

In order to investigate the species in the FLiNaK–CeF₃ and FLiNaK–CeF₃–Li₂O melts, *in situ* high temperature Raman spectroscopy was used with the aid of density functional theory (DFT) calculation. In molten FLiNaK, the CeF₆³⁻ octahedra affected by alkali cations were identified to be the predominant species. Binuclear cerium oxyfluoride anions Ce₂OF₈⁴⁻ and Ce₂OF₁₀⁶⁻ were formed after adding O²⁻ into the molten FLiNaK–CeF₃ (20 mol%) mixtures. Both of these two species were predicted to have Ce–O–Ce geometries with two CeF₄/CeF₅ moieties bridged by a single oxygen atom.

KEY WORDS

cerium fluoride, DFT, *in situ* high temperature, molten salt, oxyfluoride

1 | INTRODUCTION

Cerium fluorides are widely used in technical fields, especially the molten state applied in electrolytic process for the production Ce–Al alloys,^[1,2] in pyrochemical processes for nuclear wastes recycling,^[3,4] and in the molten salt reactor technology.^[5,6] In addition, the chemical properties of cerium fluorides are similar to the actinides fluorides making them particularly useful as models for studying the speciation of radioactive actinides, and the molten FLiNaK (46.5-mol% LiF, 11.5-mol% NaF, and 42.0-mol% KF) is used as a solvent.^[7,8] Nevertheless, moisture absorption and material corrosion bring in limitedly soluble oxygen, which accumulates into the sediment. As a result, an insoluble solid oxide phase which is the undesirable form in melts, spoils the neutron balance in the reactor, and even further cause a local increase in radioactivity.^[9] In order to predict the behavior of molten fluoride and oxyfluoride, the local structure of the melts, which is related to their physical and chemical properties, should be studied.^[10] And this

work also has great guiding significance for studying the behavior of the fission products (FPs) fluoride, which are generated from fuel salts in the operation of the molten salt reactor.

Experimental investigations regarding the structure of lanthanide fluorides in molten salts have been carried out.^[11] A series of molten KF–LnF₃ (Ln=La, Ce, Nd, Sm, Dy, Yb) mixtures has been studied by Raman spectroscopy. LnF₆³⁻ octahedra were proved to be the predominant anions at the mole fraction of X_{LnF₃} ≤ 0.25, and the distorted LnF₆³⁻ octahedra were bound by bridging fluoride (F₅Ln–F–LnF₅) at the mole fractions of X_{LnF₃} above 0.25.^[12] Nuclear magnetic resonance (NMR) and extended X-ray absorption fine structure (EXAFS) spectroscopy were also applied to the molten LiF–LaF₃ systems to study the effect of temperature on the melt compositions^[13,14]; three different anions were identified, that is, LaF₆³⁻, LaF₇⁴⁻, and LaF₈⁵⁻.^[15] Furthermore, density functional theory (DFT) calculations were performed on LaF₆³⁻ anion and compared with the experimental vibrational spectral data.^[16] Several kinds of

lanthanum oxyfluoride $\text{LaO}_x\text{F}_y^{3-x-y}$ anions in melt salts have also been studied.^[17,18] For the related research on lanthanide oxyfluoride, in addition to lanthanum oxyfluoride, there were only relevant reports on neodymium and lutetium oxyfluorides using Raman spectroscopy.^[19,20] Combined with these above studies, the structural information of fluorides in the melt has been obtained by experimental and theoretical methods, but these studies were mainly focused on lanthanum fluoride, and so far, to the best of our knowledge, no study has been devoted to investigate the cerium fluoride and oxyfluoride species in molten salt. Raman spectroscopy has been widely recognized as one of the key methods to study the microstructure of molten salt with the aid of theoretical calculations.^[21,22]

Hence, the species presented in molten FLiNaK-CeF_3 with different CeF_3 concentrations were examined by in situ high temperature Raman spectroscopy combined with DFT calculations. Because oxide can significantly alter the properties of molten salt,^[23–25] the influence of oxygen and the mechanism of forming oxyfluoride in the FLiNaK-CeF_3 melt are investigated by adding Li_2O into the molten salts.

2 | EXPERIMENTAL

The FLiNaK samples were prepared by mixing LiF (99.99%, Sigma-Aldrich), NaF (99.99%, Sigma-Aldrich), and KF (99.99%, Sigma-Aldrich) in a glassy carbon crucible using the method reported previously.^[26,27] The oxygen contents in these eutectics were less than 300 ppm (measured by LECO O836 oxygen analyzer). The molten FLiNaK-CeF_3 and $\text{FLiNaK-CeF}_3\text{-Li}_2\text{O}$ samples were prepared by the following procedures: Firstly, the CeF_3 (99.99%, Sigma-Aldrich) and Li_2O (97%, Sigma-Aldrich), vacuum dried for 8 h at 473 K, were mixed with alkali metal fluorides at a specific molar ratio; then, the mixture was placed in a platinum crucible, which was heated to a certain temperature by a Linkam TS1000 temperature-controlled hotstage (accuracy: ± 1 K) under flowing argon condition for spectral acquisition. All the above chemicals were handled in an argon glove box with oxygen and water contents less than 1 ppm.

Raman spectra of the samples were recorded by a Raman spectrometer (Horiba Jobin-Yvon LabRAM HR 800), which was equipped with charge-coupled device (CCD) detector and the 532-nm solid state laser. The spectral resolution was less than 1.0 cm^{-1} . To ensure that the samples were homogenous, each sample was tested at three different locations.

3 | COMPUTATIONAL

In order to optimize the geometry and perform wavenumber calculations, the DFT/B3LYP functional was employed,^[28,29] and different basis sets were used for the different elements (the 6-311+G[d] basis set: F, O; the SDD basis set: Ce).^[30–35] The DFT calculations used the Gaussian 09 package.^[36] The DFT calculation has been proved to be effective and feasible in predicting the structure of the ions in the molten salts,^[37–39] although part of them are electronically or thermodynamically unstable. In addition, the M06, BP86 functionals, and Hartree-Fock calculation were also employed for geometric optimization and wavenumber prediction in Figure S1.^[40–43] However, the calculated Raman spectra of CeF_6^{2-} are quite different with each other. The spectrum predicted by DFT/B3LYP functional shows a better fit with the experimental result and is adopted for the following calculation. The geometrical parameters were fully optimized, and the harmonic wavenumbers were obtained by analyzing the optimized structures. Furthermore, zero-point energy corrections were applied for the relative electronic energy calculations.

4 | RESULTS AND DISCUSSION

4.1 | Binary cerium fluoride anions in molten FLiNaK

Figure 1 shows the Raman spectra of CeF_3 with two different concentrations (10 and 20 mol%) in molten FLiNaK . No obvious bands of molten FLiNaK were observed,^[44] while the Rayleigh wing extended beyond

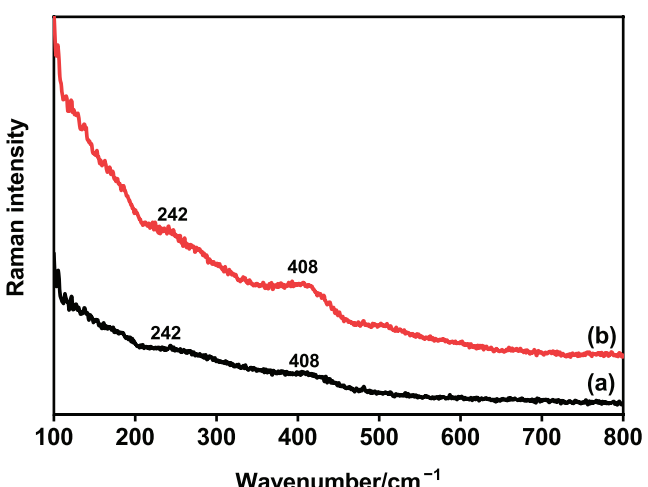


FIGURE 1 Raman spectra of the FLiNaK melts with different CeF_3 concentrations at 973 K: (a) 10 and (b) 20 mol% CeF_3 [Colour figure can be viewed at wileyonlinelibrary.com]

300 cm^{-1} .^[45] This background in the low-wavenumber region was due to polarizability changes associated with the short-lived ion pairs.^[46,47] There were two weak bands observed at 242 and 408 cm^{-1} , after dissolving CeF_3 (10 mol\%) in molten FLiNaK . The intensities increased when the concentration of CeF_3 reached 20 mol\% , and no band shift was observed, which was almost the same as the previous studies on the KF-CeF_3 (10 and 20 mol\%) melts.^[12] Both these two bands were assigned to the poorly defined octahedral CeF_6^{3-} anion. Further increasing the concentration of CeF_3 led to the formation of fluorine-bridged distorted CeF_6^{3-} octahedra.^[10] These assignments were based on the structure in solid state, but it was not always in accordance with the structure in melt.^[44,48] Therefore, further confirmation is required.

For the assignment of the two bands observed in the FLiNaK-CeF_3 melt, DFT calculations at the B3LYP level were carried out on the cerium fluoride anions. No band was observed for bridging fluoride stretching, while candidate anions in the form of $\text{CeF}_n^{(n-3)-}$ ($n = 4-7$) were considered. All of these doublet anions were predicted to be geometrically stable as shown in Figure 2. The isomers for CeF_5^{2-} were optimized to be stable with C_{4v} and D_{3h} symmetries, and the isomer with D_{3h} symmetry was less stable than that with C_{4v} symmetry by 3.3 kcal/mol . All these geometries were optimized with Ce–F bond lengths of around 2.3 \AA . The optimized geometries of LaF_4^- , LaF_5^{2-} , and LaF_6^{3-} reported previously were extremely close to the cerium fluorides anions at the same level of theory.^[14,49]

The calculated Raman spectra of the $\text{CeF}_n^{(n-3)-}$ ($n = 4-7$) anions are shown in Figure 3, and the calculated wavenumbers are listed in Table S1. The assignment of the experimental Raman bands of the FLiNaK-CeF_3 melts is carried out by comparing the calculated and the experimental wavenumbers and relative intensities.^[50,51] The calculated bands of the Ce–F symmetrical stretching were all around 400 cm^{-1} , whereas

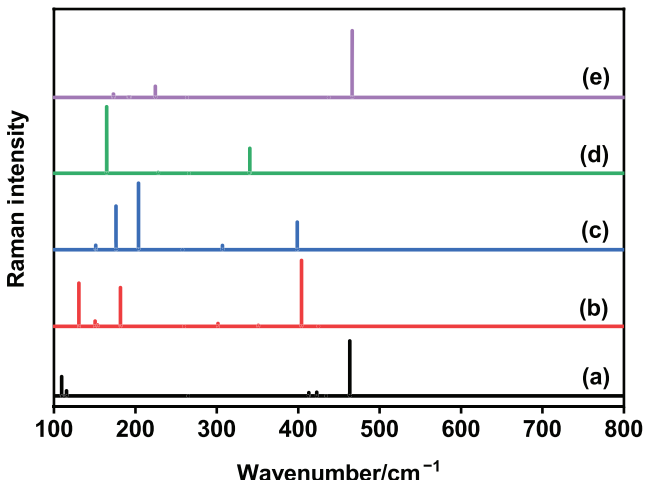


FIGURE 3 Calculated Raman spectra of $\text{CeF}_n^{(n-3)-}$ ($n = 4-7$) anions: (a) CeF_4^- (C_1), (b) CeF_5^{2-} -A (C_{4v}), (c) CeF_5^{2-} -B (D_{3h}), (d) CeF_6^{3-} (O_h), and (e) CeF_7^{4-} (C_{2v}) [Colour figure can be viewed at wileyonlinelibrary.com]

no Raman band was found in the low-wavenumber region around 200 cm^{-1} for the CeF_4^- and CeF_7^{4-} anions. In addition, two intense bands were predicted for the CeF_5^{2-} -A (C_{4v}) located at 176 , 204 cm^{-1} and the CeF_5^{2-} -B (D_{3h}) located at 131 , 182 cm^{-1} . In comparison with the experimental values, only one band was observed at 242 cm^{-1} , which is not consistent with CeF_5^{2-} anions. A better assignment can be reached with taking the CeF_6^{3-} anion into account; both the position and relative intensity are consistent. The observed 242 cm^{-1} band is assigned to $\nu_5(T_{2g})$ (164 cm^{-1}), and 408 cm^{-1} band is assigned to $\nu_1(A_{1g})$ (340 cm^{-1}) of CeF_6^{3-} . In addition to the isolated anions, geometric optimization and wavenumber calculations were also carried out on the neutral M_3CeF_6 ($\text{M}=\text{Li, Na, K}$) ion pairs where alkali cations were included for comparison in Figures S2 and S3. The $\text{Na}_3\text{CeF}_6/\text{K}_3\text{CeF}_6$ ion pair seems to offer a reasonable match, and it suggests that the Raman spectra are actually affected by alkali metal cations. It should be

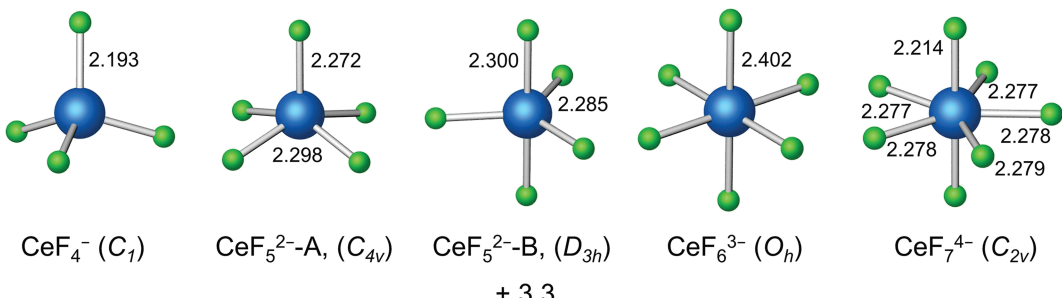


FIGURE 2 Optimized geometries (bond lengths in \AA) of $\text{CeF}_n^{(n-3)-}$ ($n = 4-7$) at the B3LYP level of theory (Ce: blue, F: green). CeF_4^- possesses an approximate D_{2d} symmetry. CeF_7^{4-} possesses an approximate D_{5h} symmetry. The energy (kcal/mol) is relative to the most stable isomer A [Colour figure can be viewed at wileyonlinelibrary.com]

noting that the theoretical Raman bands are lower than the observed results in a molten salt environment, without considering the counterions.^[16,52] The anions with gas phase model can be employed to explain the speciation in molten salt, and it is in good agreement with the results reported both in high temperature and low temperature (ionic liquid) molten salts.^[44,53] It is worth noting that the discrepancies between experimental and theoretical wavenumbers of cerium fluoride anions are quite significant, which can be attributed to differences between melt and gas phase. This can be related to marginal electronic stability of CeF_6^{3-} , which causes its properties to be strongly affected by the molten salt environment.^[16]

4.2 | Ternary cerium oxyfluoride anions in molten FLiNaK

The O^{2-} was introduced by adding Li_2O into the molten FLiNaK- CeF_3 (20 mol%) mixtures. The Raman spectra are plotted as a function of the Li_2O molar fraction at 973 K in Figure 4. As the Li_2O content increased from 5 mol%, the weak bands at 242 and 408 cm^{-1} assigned to CeF_6^{3-} were not observed anymore. Simultaneously, a sharp band at 451 cm^{-1} and a broad band at 354 cm^{-1} appeared. When the concentration of Li_2O reached 10 mol%, the broad band at 354 cm^{-1} blue-shifted to 376 cm^{-1} , and another band kept the position unchanged. In addition, both of these two bands increased in intensity as expected. The difference in shift behavior of these two bands suggested that at least two species existed in the melts and overlapped in the bands

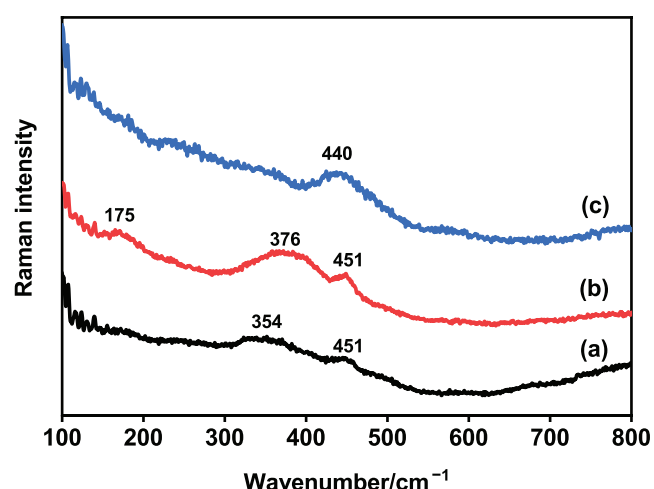


FIGURE 4 Raman spectra of the FLiNaK- CeF_3 (20 mol%) melts with increasing concentrations of Li_2O at 973 K: (a) 5 mol% Li_2O , (b) 10 mol% Li_2O , and (c) 20 mol% Li_2O [Colour figure can be viewed at wileyonlinelibrary.com]

located around 354 and 376 cm^{-1} . As more Li_2O was added into the melt, these two bands disappeared with the observation of one broad band at 440 cm^{-1} when the concentration of Li_2O reached 20 mol%. Further increasing the concentration of Li_2O generated insoluble solid on the surface of the melt, and no observable band of the melts was found in the Raman spectrum.

To identify the structure of the oxyfluoride caused by Li_2O addition, DFT/B3LYP calculations were carried out. Geometry optimization was first initiated with the $\text{CeOF}_x^{(x-1)-}$ ($x = 2-6$) singlet anions as shown in Figure 5. The Ce–O bond is elongated from 1.9 to 2.4 \AA as more F^- is coordinated to the central cerium atom, and the same situation occurred to the Ce–O bonds (1.917 – 2.435 \AA). Because the structure of the molten FLiNaK- CeF_3 mixtures at high dilution was predominant by the octahedral CeF_6^{3-} with O_h symmetry, spectral features indicate that the oxyfluoride complexes should be similar to the CeF_6^{3-} anion. Probable oxyfluoride species conforming to the spectral data were the mononuclear CeOF_4^{3-} , CeOF_5^{4-} , and the binuclear $\text{Ce}_2\text{OF}_8^{4-}$, $\text{Ce}_2\text{OF}_9^{5-}$, and $\text{Ce}_2\text{OF}_{10}^{6-}$ anions. As to the mononuclear $\text{CeOF}_x^{(x-1)-}$ anions, the bands of terminal Ce–O stretching mode were all above 500 cm^{-1} (Figure 6 and Table S2). It suggested that mononuclear cerium oxyfluoride anions are not present in molten fluoride.

The dinuclear oxyfluorides $\text{Ce}_2\text{OF}_y^{(y-4)-}$ with the value of y varying between 5 and 10 were then carried out as shown in Figure 7. It is to be expected that the anions will have two tetrahedra connected through a bridging oxygen atom. Although a bent Ce–O–Ce bond was expected, all the structures were optimized to linear Ce–O–Ce configurations except Ce_2OF_5^- anion. The Ce–O bond lengths range from 1.990 to 2.343 \AA , which are around the typical Ce–O single bonds.^[54] The Ce–F bond lengths are all around 2.2 \AA . Figure 8 shows the calculated Raman bands for the $\text{Ce}_2\text{OF}_y^{(y-4)-}$ isomers with $y = 5-10$, and Table S3 shows the calculated wavenumbers. The $\text{Ce}_2\text{OF}_9^{5-}$ anion is predicted not to be present due to the intense band of $\nu_1(A_1)$ located at 658 cm^{-1} , whereas the observed Raman bands are all below 500 cm^{-1} . The intense bands of Ce_2OF_5^- and $\text{Ce}_2\text{OF}_6^{2-}$ are located at 466 and 414 cm^{-1} , respectively. Because the observed band at 451 cm^{-1} was related to the band at 354 cm^{-1} , the bands cannot be assigned to either Ce_2OF_5^- or $\text{Ce}_2\text{OF}_6^{2-}$ with only one intense band. By comparison with the experimental Raman spectra, the observed bands at 354 and 451 cm^{-1} are better reproduced by the calculated wavenumbers of 426 ($\nu_1[A_1]$) and 332 cm^{-1} ($\nu_{16}[E]$) for $\text{Ce}_2\text{OF}_{10}^{6-}$ with D_4 symmetry, whereas the observed Raman band at 376 cm^{-1} is matched by the wavenumber of 336 cm^{-1} ($\nu_9[B_3]$) for $\text{Ce}_2\text{OF}_8^{4-}$ with D_2 symmetry. Moreover, the

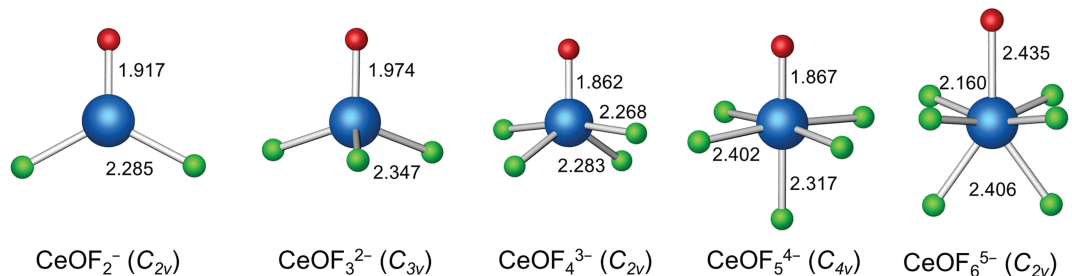


FIGURE 5 Optimized geometries (bond lengths in Å) of $\text{CeOF}_x^{(x-1)-}$ ($x = 2-6$) anions at the B3LYP level of theory (Ce: blue, F: green, O: red) [Colour figure can be viewed at wileyonlinelibrary.com]

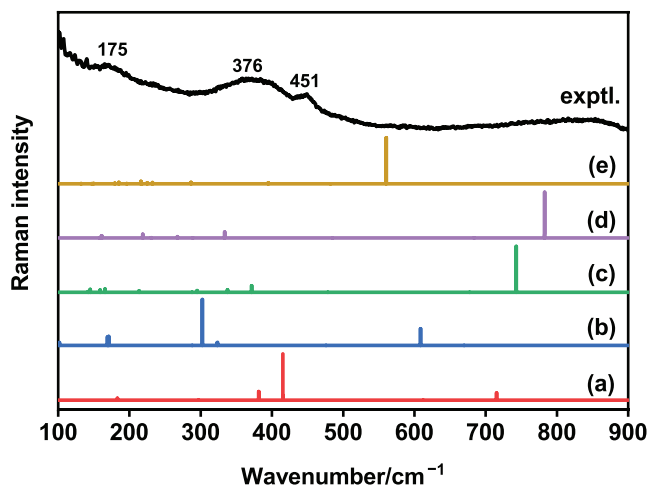


FIGURE 6 Experimental Raman spectrum of molten FLiNaK– CeF_3 (20 mol%) containing 10 mol% Li_2O (top) and calculated Raman spectra of $\text{CeOF}_x^{(x-1)-}$ anions: (a) CeOF_2^- , (b) CeOF_3^{2-} , (c) CeOF_4^{3-} , (d) CeOF_5^{4-} , and (e) CeOF_6^{5-} [Colour figure can be viewed at wileyonlinelibrary.com]

observed band at 175 cm^{-1} is due to the sum of multiple Ce–F bending modes.

The dissolution mechanism and effect of O^{2-} in the FLiNaK– CeF_3 melt are investigated by in situ high temperature Raman spectroscopic and theoretical results. When Li_2O was added into the FLiNaK– CeF_3 (20 mol%) melts, $\text{Ce}_2\text{OF}_8^{4-}$ and $\text{Ce}_2\text{OF}_{10}^{6-}$ anions were formed as described in Reactions 1 and 2. The proportion of these two anions in the melt changed according to the O^{2-} content. When the concentration of Li_2O was low ($\leq 5 \text{ mol \%}$), $\text{Ce}_2\text{OF}_{10}^{6-}$ anion was the dominating species in the melt. The content of $\text{Ce}_2\text{OF}_8^{4-}$ gradually increased with Li_2O increased to 10 mol%. The broad band at around 354 cm^{-1} was firstly formed at the cost of CeF_6^{3-} and assigned to the sum of $\text{Ce}_2\text{OF}_{10}^{6-}$ and $\text{Ce}_2\text{OF}_8^{4-}$ anions. Both of these two oxyfluorides are predicted to possess Ce–O–Ce geometries. A blue shift of the band at 354 – 376 cm^{-1} was observed and a new band appearing at 175 cm^{-1} when the concentration of Li_2O reached 10 mol

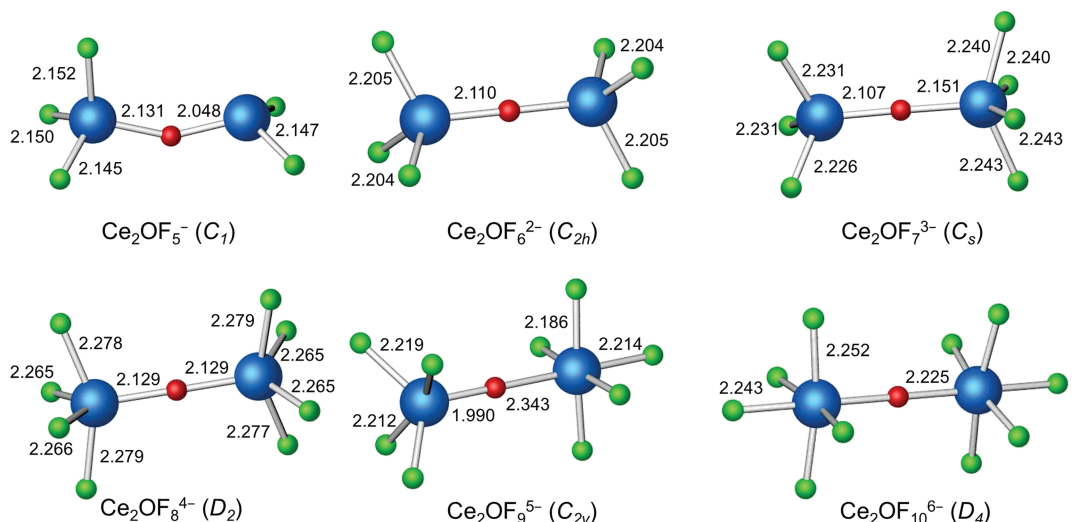


FIGURE 7 Optimized geometries (bond lengths in Å) of $\text{Ce}_2\text{OF}_y^{(y-4)-}$ ($y = 5-10$) at the B3LYP level of theory (Ce: blue, F: green, O: red) [Colour figure can be viewed at wileyonlinelibrary.com]

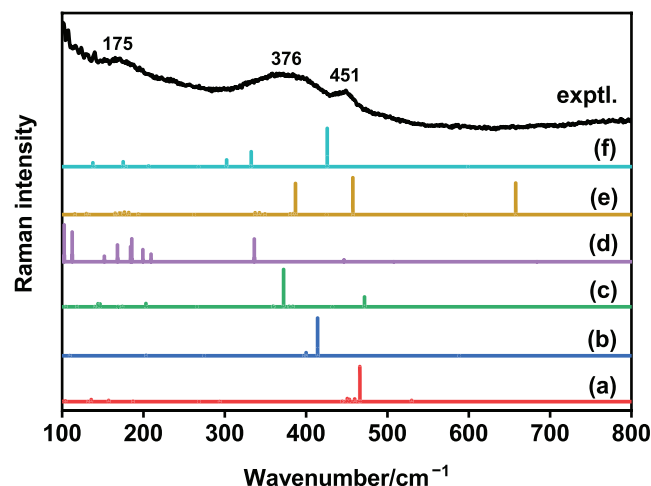


FIGURE 8 Experimental Raman spectrum of molten FLiNaK–CeF₃ (20 mol%) containing 10 mol% Li₂O (top) and calculated Raman spectra of dinuclear Ce₂OF_y^{(y-4)-} anions: (a) Ce₂OF₅⁴⁻, (b) Ce₂OF₆²⁻, (c) Ce₂OF₇³⁻, (d) Ce₂OF₈⁴⁻, (e) Ce₂OF₉⁵⁻, and (f) Ce₂OF₁₀⁶⁻ [Colour figure can be viewed at wileyonlinelibrary.com]

%. Such variation in relative intensity indicated that more Ce₂OF₈⁴⁻ was formed while the content of Ce₂OF₁₀⁶⁻ decreased. According to the binding energies of the similar Zr₂OF_y^{(y-6)-} species,^[55] Ce₂OF₈⁴⁻ seemed to be more stable than Ce₂OF₁₀⁶⁻ with the increasing content of O²⁻. Further increasing the concentration of Li₂O resulted in only one obvious band arising at 440 cm⁻¹ in the spectrum. It is speculated that the 440 cm⁻¹ can be attributed to the similar trigonal Ce₂O₃ in which four-coordinate cerium ions are bridged by two oxygen atoms and form a network structure.^[56–58] Therefore, the Ce₂O₂F_z^{(z-2)-} (z = 3–6) anions containing a Ce₂O₂ ring were optimized in Figure S4. The computed Raman bands for all the Ce₂O₂F_z^{(z-2)-} anions are shown in Figure S5. The intense band observed at 440 cm⁻¹ is closest to the symmetric Ce–F stretch of Ce₂O₂F₄²⁻, which is predicted at 378 cm⁻¹. In addition, the weak band observed at 578 cm⁻¹ corresponds to the band computed at 511 cm⁻¹ due to the symmetric Ce–O stretch.



5 | CONCLUSIONS

Basic structural species in the molten FLiNaK–CeF₃ and FLiNaK–CeF₃–Li₂O at 973 K were determined by high

temperature Raman spectroscopy with the help of theoretical calculations. With the effect of the alkali cations, the CeF₆³⁻ anion was predicted to be the predominant species in the FLiNaK–CeF melt.

As Li₂O was dissolved in molten FLiNaK–CeF₃ (5 mol%), a series of new bands increased at 354 and 451 cm⁻¹ at the expense of CeF₆³⁻. Further increasing the concentration of Li₂O caused the band at 354 cm⁻¹ to shift to 376 cm⁻¹, and a weak band appeared at 175 cm⁻¹. These bands are assigned to Ce₂OF₈⁴⁻ and Ce₂OF₁₀⁶⁻ anions, respectively, according to the concentration of Li₂O (5 and 10 mol%). For these two cerium oxyfluoride anions, two CeF₃ moieties are joint by a bridging oxygen atom in the form of a Ce–O–Ce geometry. When 20 mol% Li₂O was added, only one intense band located at 440 cm⁻¹ appeared and was assigned to the cerium oxyfluoride, which is similar to the trigonal Ce₂O₃. The mechanisms of the microstructural evolution in the molten FLiNaK–CeF₃–Li₂O are proposed. The Ce₂OF₈⁴⁻ and Ce₂OF₁₀⁶⁻ anions can be regarded as the intermediates between cerium fluoride anions and insoluble cerium oxides.

ACKNOWLEDGEMENTS

This work was supported by the Strategic Priority Research Program and Frontier Science Key Program of the Chinese Academy of Sciences (Grants XDA02030000 and QYZDY-SSW-JSC016).

ORCID

Rongrong Cui <https://orcid.org/0000-0002-6799-894X>
Chenyang Wang <https://orcid.org/0000-0002-7295-6904>

REFERENCES

- [1] A. Inoue, K. Ohara, T. Masumoto, *Japan. J. Appl. Phys.* **1988**, 27, L736. <https://doi.org/10.1143/jjap.27.1736>
- [2] O. P. Bansal, J. A. Morrison, *Mater. Res. Bull.* **1975**, 10, 1181. [https://doi.org/10.1016/0025-5408\(75\)90024-0](https://doi.org/10.1016/0025-5408(75)90024-0)
- [3] M. Gibilaro, L. Massot, P. Chamelot, P. Taxil, *Electrochim. Acta* **2009**, 54, 5300. <https://doi.org/10.1016/j.electacta.2009.01.074>
- [4] P. Taxil, L. Massot, C. Nourry, M. Gibilaro, P. Chamelot, L. Cassayre, *J. Fluorine Chem.* **2009**, 130(1), 94. <https://doi.org/10.1016/j.jfluchem.2008.07.004>
- [5] O. Beneš, R. J. M. Konings, *J. Nucl. Mater.* **2013**, 435, 164.
- [6] C. F. Baes Jr., *J. Nucl. Mater.* **1974**, 51, 149.
- [7] Z. Dai, *Molten Salt Reactors and Thorium Energy*, Woodhead Publishing, England, Cambridge **2017**, 531.
- [8] C. N. A. C. Z. Bahri, W. M. Al-Areqi, M. I. F. M. Ruf, A. A. Majid, *AIP Conf. Proc.* **2017**, 1799, 040008.
- [9] R. Pshenichny, A. Omelchuk, *Russ. J. Inorg. Chem.* **2012**, 57, 115.
- [10] A. F. Vik, V. Dracopoulos, G. N. Papathodorou, T. Østvold, *J. Chem. Soc., Dalton Trans.* **2001**, 2164. <https://doi.org/10.1039/B101528L>

- [11] A.-L. Rollet, M. Salanne, *Annu. Rep. Prog. Chem., Sect. C: Phys. Chem.* **2011**, *107*, 88.
- [12] V. Dracopoulos, B. Gilbert, G. Papatheodorou, *J. Chem. Soc., Faraday Trans.* **1998**, *94*, 2601. <https://doi.org/10.1039/a802812e>
- [13] A.-L. Rollet, A. Rakhmatullin, C. Bessada, *Int. J. Thermophys.* **2005**, *26*, 1115.
- [14] A.-L. Rollet, C. Bessada, A. Rakhmatoulline, Y. Auger, P. Melin, M. Gailhanou, D. Thiaudiére, *C. R. Chim.* **2004**, *7*, 1135.
- [15] A.-L. Rollet, S. Godier, C. Bessada, *Phys. Chem. Chem. Phys.* **2008**, *10*, 3222. <https://doi.org/10.1039/b719158h>
- [16] M. Gutowski, A. I. Boldyrev, J. Simons, J. Rak, J. Błażejowski, *J. Am. Chem. Soc.* **1996**, *118*, 1173.
- [17] E. Stefanidaki, G. M. Photiadis, C. G. Kontoyannis, A. F. Vik, T. Østvold, *J. Chem. Soc., Dalton Trans.* **2002**, *11*, 2302. <https://doi.org/10.1039/b111563b>
- [18] A.-L. Rollet, E. Veron, C. Bessada, *J. Nucl. Mater.* **2012**, *429*, 40.
- [19] A.-L. Rollet, H. Matsuura, C. Bessada, *Dalton Trans.* **2015**, *44*, 522.
- [20] X. Liu, Y. Li, B. Wang, C. Wang, *Spectrochim. Acta a* **2021**, *251*, 119435.
- [21] S. Zhang, S. Wan, Y. Zeng, S. Jiang, X. Gong, *Inorg. Chem.* **2019**, *58*, 5025.
- [22] Y. Li, X. Liu, B. Wang, C. Wang, *J. Mol. Liq.* **2021**, *325*, 115208.
- [23] V. I. Konstantinov, E. G. Polyakov, P. T. Stangrit, *Electrochim. Acta* **1981**, *26*, 445.
- [24] E. W. Dewing, J. Thonstad, *Metall. Mater. Trans. B* **1997**, *28*, 1089. <https://doi.org/10.1007/s11663-997-0063-x>
- [25] S. Mukherjee, S. Dash, S. K. Mukerjee, K. L. Ramakuma, *J. Nucl. Mater.* **2015**, *465*, 604.
- [26] M. H. Brooker, R. W. Berg, J. H. von Barner, N. J. Bjerrum, *Inorg. Chem.* **2000**, *39*, 3682.
- [27] J. H. von Barner, E. Christensen, N. J. Bjerrum, B. Gilbert, *Inorg. Chem.* **1991**, *30*, 561.
- [28] A. D. Becke, *J. Chem. Phys.* **1993**, *98*, 5648.
- [29] C. Lee, W. Yang, R. G. Parr, *Phys. Rev. B* **1988**, *37*, 785.
- [30] R. Krishnan, J. S. Binkley, R. Seeger, J. A. Pople, *J. Chem. Phys.* **1980**, *72*, 650.
- [31] M. Dolg, H. Stoll, A. Savin, H. Preuss, *Theor. Chim. Acta* **1989**, *75*, 173.
- [32] M. Dolg, H. Stoll, H. Preuss, *J. Chem. Phys.* **1989**, *90*, 1730.
- [33] M. Dolg, P. Fulde, W. Kuechle, C.-S. Neumann, H. Stoll, *J. Chem. Phys.* **1991**, *94*, 3011.
- [34] M. Dolg, H. Stoll, H. Preuss, *Theor. Chem. Acc.* **1993**, *85*, 441.
- [35] X. Y. Cao, M. Dolg, *J. Chem. Phys.* **2001**, *115*, 7348. <https://doi.org/10.1063/1.1406535>
- [36] M. J. Frisch, G. W. Trucks, H. B. Schlegel, G. E. Scuseria, M. A. Robb, J. R. Cheeseman, G. Scalmani, V. Barone, B. Mennucci, G. A. Petersson, Gaussian 09, revision A.01, Gaussian, Inc., Wallingford, CT **2009**.
- [37] M. H. Brooker, R. W. Berg, J. H. von Barner, N. J. Bjerrum, *Inorg. Chem.* **2000**, *39*, 4725.
- [38] C. Wang, X. Chen, R. Wei, Y. Gong, *J. Phys. Chem. B* **2020**, *124*, 6671.
- [39] C. Wang, X. Chen, Y. Gong, *J. Phys. Chem. B* **2021**, *125*, 1640.
- [40] C. C. J. Roothaan, *Rev. Mod. Phys.* **1951**, *23*, 69.
- [41] A. D. Becke, *Phys. Rev. A: At., Mol., Opt. Phys.* **1988**, *38*, 3098.
- [42] J. P. Perdew, *Phys. Rev. B: Condens. Matter Mater. Phys.* **1986**, *33*, 8822.
- [43] A. D. Becke, *J. Chem. Phys.* **1997**, *107*, 8554.
- [44] S. E. Bae, T. S. Jung, Y. H. Cho, J. Y. Kim, K. Kwak, T. H. Park, *Inorg. Chem.* **2018**, *57*, 8299.
- [45] J. Dai, H. Han, Q. Li, P. Huai, *J. Mol. Liq.* **2016**, *213*, 17.
- [46] G. N. Papatheodorou, V. Dracopoulos, *Chem. Phys. Lett.* **1995**, *241*, 345.
- [47] G. N. Papatheodorou, S. G. Kalogrianitis, T. G. Mihopoulos, E. A. Pavlatou, *J. Chem. Phys.* **1996**, *105*, 2660.
- [48] V. Dracopoulos, J. Vagelatos, G. Papatheodorou, *J. Chem. Soc. Dalton Trans.* **2001**, *7*, 1117.
- [49] M. Gutowski, A. I. Boldyrev, J. V. Ortiz, J. Simons, *J. Am. Chem. Soc.* **1994**, *116*, 9262.
- [50] N. E. Heimer, R. E. del Sesto, Z. Meng, J. S. Wilkes, W. R. Carpera, *J. Mol. Liq.* **2006**, *124*, 84.
- [51] W. R. Carper, K. Langenwalter, N. S. Nooruddin, M. J. Kullman, D. Gerhard, P. Wasserscheid, *J. Phys. Chem. B* **2009**, *113*, 2031.
- [52] A. V. Voit, E. I. Voit, V. I. Sergienko, *J. Struct. Chem.* **1999**, *40*, 838.
- [53] M. S. Sitze, E. R. Schreiter, E. V. Patterson, R. G. Freeman, *Inorg. Chem.* **2001**, *40*, 2298.
- [54] N. C. Baenziger, J. R. Holden, G. E. Knudson, A. I. Popov, *J. Am. Chem. Soc.* **1954**, *76*, 4734.
- [55] A. S. Vorob'ev, A. V. Suzdal'tsev, A. E. Galashev, *Russian Metallurgy (Metally)* **2019**, *2019*, 781.
- [56] B. Wu, M. Zinkevich, F. Aldinger, D. Wen, L. Chen, *J. Solid State Chem.* **2007**, *180*, 3280.
- [57] M. Mikami, S. Nakamura, *J. Alloy. Compd.* **2006**, *408-412*, 687.
- [58] L. Brugnoli, A. M. Ferrari, B. Civalleri, A. Pedone, M. C. Menziani, *J. Chem. Theory Comput.* **2018**, *14*, 4914.

SUPPORTING INFORMATION

Additional supporting information may be found online in the Supporting Information section at the end of this article.

How to cite this article: Cui R, Wang C. In situ high temperature Raman and DFT analysis of cerium fluoride and oxyfluoride structures in molten FLiNaK. *J Raman Spectrosc.* 2021;52: 1148–1154. <https://doi.org/10.1002/jrs.6093>